Diverse phage defence systems define West African South American pandemic *Vibrio cholerae*

David W. Adams[1,2]*, Milena Jaskólska[1], Alexandre Lemopoulos[1], Sandrine Stutzmann[1], Laurie Righi[1], Loriane Bader[1] and Melanie Blokesch[1,2]*

[1]Laboratory of Molecular Microbiology, Global Health Institute, School of Life Sciences, Station 19, EPFL-SV-UPBLO, Ecole Polytechnique Fédérale de Lausanne (EPFL), CH-1015 Lausanne, Switzerland.

[2]These authors contributed equally.

*Corresponding authors: david.adams@epfl.ch and melanie.blokesch@epfl.ch

Summary

Our understanding of the factors underlying the evolutionary success of different lineages of pandemic *Vibrio cholerae* remains incomplete. Interestingly, two unique genetic signatures define the West African South American (WASA) lineage of *V. cholerae* responsible for the 1991-2001 Latin American cholera epidemic. Here we show these signatures encode diverse anti-phage defence systems. Firstly, the WASA-1 prophage encodes a 2-gene abortive-infection system WonAB that renders the lineage resistant to the major predatory *vibrio*phage ICP1, which alongside other phages, restricts cholera epidemics and has potential for use in prophylaxis. Secondly, the unique set of genes on *Vibrio* seventh pandemic island II encodes an unusual modification-dependent restriction system and a new type of the Shedu defence family. Taken together, we propose that these anti-phage defence systems have likely contributed to the success of a major epidemic lineage of the ongoing seventh cholera pandemic.

24 The ability of lytic bacteriophages to rapidly devastate bacterial populations has driven the evolution
25 of multiple layers of defence, including a diverse array of specialised anti-phage defence systems[1].
26 Bacteriophages also have the potential to affect bacterial pathogenesis. Indeed, bacteriophage
27 predation is thought to limit the duration and severity of cholera epidemics, as well as affecting
28 individual patient outcomes[2-5]. Sampling of cholera patients has revealed that the O1 El Tor strains of
29 *Vibrio cholerae* responsible for the ongoing seventh cholera pandemic (7PET) consistently co-occur
30 with three lytic phages ICP1, 2 and 3, with ICP1 being most frequently isolated[6,7]. Furthermore, the
31 demonstration that a cocktail of ICP1-2-3 can prevent cholera in animal infection models has led to
32 renewed interest in using phages as a prophylactic treatment[8]. There is therefore an urgent need to
33 understand the mechanisms by which *V. cholerae* defends against these viruses.
34 Since 1961 7PET strains have spread out from the Bay of Bengal in a series of three distinct but
35 overlapping waves[9]. Importantly, from Wave 2 onwards strains acquired SXT/R391 integrative and
36 conjugative elements (SXT-ICE), which in addition to carrying multiple antibiotic resistance genes,
37 encode a variable anti-phage defence hotspot that in the globally dominant SXT-ICE harbours either
38 BREX or Restriction-Modification systems active against ICP1-3[9,10]. Additionally, a family of viral
39 satellites, the Phage-inducible chromosomal island-like elements (PLE), also occur sporadically and
40 specifically parasitise ICP1 infection to mediate their own transmission[11,12]. Notably, these elements
41 exemplify the co-evolutionary arms race of defence and counter-defence between bacterial hosts and
42 their viral predators, with the emergence of resistant ICP1 selecting for either alternative SXT-ICE
43 carrying new defence systems or new PLE[10,13]. In contrast, how 7PET strains that lack SXT-ICE/PLE
44 defend against these phages remains unknown. Given their ubiquitous nature and ability to shape
45 epidemics, we hypothesised that these strains likely contained additional defence systems with activity
46 against ICP1-3.
47
48 **WASA-1 prophage renders Peruvian strains resistant to ICP1**
49 To test this hypothesis, we challenged a set of intensively studied wave 1 strains that lack SXT-ICE/PLE
50 with a well-characterised collection of ICP1-3 phages. All strains showed the expected sensitivities to

ICP2 and ICP3 (Fig. 1A and Extended Data Fig. 1A). Unexpectedly, however, the widely used model strain A1552 – a Peruvian isolate – was completely resistant to all tested ICP1 isolates spanning a twenty-seven-year period, displaying a 10^5-fold reduction in plaque formation and a similar defect in ICP1 replication (Fig. 1A and Extended Data Fig. 1A-C). Notably, the contemporary Peruvian strains C6706 and C6709 also behaved similarly. ICP1 resistance was independent of the *Vibrio* pathogenicity islands (VPI-1/2) and the *Vibrio* seventh pandemic islands (VSP-I/II), which together harbour multiple known anti-viral defence systems[14-21] (Extended Data Fig. 1D). Moreover, the ICP1 resistant strains were predicted to encode the same repertoire of defence systems as the ICP1 sensitive strains (table S1), suggesting that ICP1 resistance was likely due to the presence of a novel defence system(s) not recognised by the currently available prediction tools.

The Peruvian strains are members of the West African South American (WASA) lineage of 7PET *V. cholerae*[9], which was responsible for a massive cholera epidemic that started in Peru in 1991, before spreading rapidly throughout Latin America, resulting in over 1.2 million cholera cases and approximately 12,000 deaths[22]. Interestingly, phylogenetic analysis has shown that these strains originated in West Africa, where they acquired two genetic signatures that define the WASA lineage: (i) a novel set of genes on VSP-II and (ii) the WASA-1 prophage[9,23-26]. Since deletion of VSP-II had no effect on ICP1 resistance we tested strains deleted for WASA-1. Strikingly, this abolished defence against ICP1 in all tested Peruvian strains, and restored ICP1 replication to levels similar to those of a susceptible control (Fig. 1B-E). Moreover, introducing WASA-1 into non-WASA lineage strains rendered them ICP1 resistant (Extended Data Fig. 1E).

WonAB system is responsible for ICP1 defence

The WASA-1 prophage is highly conserved throughout all WASA lineage strains[9,25], and interestingly, is also found in diverse *Vibrio* spp. where it displays a broadly conserved genome encoding proteins involved in capsid/tail biogenesis, DNA replication and a recombinase (Fig. 1B, Extended Data Fig. 2A and table S2). To determine the gene(s) responsible for ICP1 defence, we used an existing RNA-seq dataset[27] to identify WASA-1 genes expressed under laboratory conditions, and then screened

78 truncations of these regions for loss of protection (Extended Data Fig. 2B). This revealed a 2-gene
79 operon (A1552VC_01233-34) encoding an ATPase and a hypothetical protein, downstream of a
80 conserved putative transcriptional regulator (A1552VC_01232) (Fig. 1B). For the reasons outlined
81 below we have renamed this operon WASA OLD-ABC ATPase Nuclease, WonAB. Strikingly, deletion of
82 *wonAB* abolished protection against ICP1. Moreover, ectopic expression of *wonAB* complemented the
83 Δ*wonAB* deletion and conferred complete protection to ICP1-sensitive non-WASA strains (Fig. 1D-E).
84 Importantly, both genes were required for protection indicating that production of WonAB is both
85 necessary and sufficient for anti-phage activity (Fig. 1F). Notably, although WonAB is unique to the
86 WASA-1 prophage found in *V. cholerae*, known defence systems could also be found at the same locus
87 in other non-cholerae WASA-1 (table S2), consistent with the observation that prophages often carry
88 anti-phage defence systems to increase the fitness of their bacterial hosts[28-30].

89 Bioinformatic analysis revealed that WonA is an ATP-binding cassette (ABC) ATPase with a
90 predicted core β-barrel like ATPase fold characteristic of the ABC-ATPase clade[31]. Motifs required for
91 ATP binding and hydrolysis (Walker A, Q-loop, ABC-signature, Walker B, D-loop and H-loop) were
92 readily identifiable (Fig. 1G and Extended Data Fig. 3A). Moreover, structural modelling confidently
93 predicted that WonA forms a dimer, in which these motifs are positioned at the dimer interface to
94 form the composite ATP-binding sites typical of ABC-ATPases[31] (Fig. 1G, Extended Data Figs. S3B and
95 S4A-B). In contrast, WonB is predicted to encode a variant of the PD-(D/E)xK nuclease fold, with the
96 highly conserved active site residues clustered together[32] (Fig. 1G and Extended Data Fig. 3C-D).
97 Variants designed to disrupt either WonA ATP-binding/hydrolysis (K34A; R182A; E300A; H333A) or
98 WonB nuclease activity (K71A) all abolished protection against ICP1, despite mostly being produced at
99 similar levels to the WT control (Fig. 1H and Extended Data Fig. 3E). Interestingly, Western blotting
100 showed that inactivating WonA ATPase activity resulted in the loss of WonB, suggesting that WonA
101 regulates or otherwise affects the stability of WonB (Extended Data Fig. 3E). Indeed, the two proteins
102 are predicted to form a complex, with WonB binding to a surface created by the dimerised C-terminal
103 extensions of WonA (Extended Data Fig. 4A-D).

104 Homologues of WonAB are found in diverse classes of mainly Gram-negative bacteria and
105 overall were present in 0.43% of bacterial genomes examined (Extended Data Fig. 3F and table S3).
106 Notably, when expressed in *Escherichia coli* WonAB displayed robust activity against all members of
107 the *Vequintavirinae* subfamily of the BASEL bacteriophage collection[33], indicating that WonAB activity
108 is not limited to ICP1 (Extended Data Fig. 5). Interestingly, WonA ATPase motifs display deviations
109 typical of the overcoming lysogenisation defect (OLD) family of ABC-ATPases[31,34] (Extended Data Fig.
110 3A). However, members of this family such as OLD, Gabija, PARIS and the related Septu, are distinct
111 from WonA in both structure and domain composition[34-39]. In contrast, WonAB appears to be closely
112 related to an operon encoding a predicted OLD-ABC ATPase and a novel version of the restriction-
113 enzyme fold (Extended Data Fig. 4), detected during a recent comprehensive *in silico* survey of ABC-
114 ATPases[31]. Moreover, homologues of this operon are found in 0.96% of bacterial genomes and
115 encompass all detected homologues of WonAB (table S3). Furthermore, WonAB also shows similarity
116 to operons with a similar organisation such as PD-T4-4 that have also recently been identified
117 (Extended Data Fig. 4), albeit with variations in the Insert 1/2 regions and C-terminal extensions of the
118 ATPase, and in some cases a distinct nuclease[29,40]. Taken together, these data suggest that WonAB is
119 part of a larger as yet uncharacterised family of ABC-ATPase sensors that are paired with nuclease
120 effectors.
121
122 **ICP1 defence occurs via lysis-independent abortive infection**
123 To gain insights into how WonAB mediates ICP1 defence we monitored the growth kinetics of ICP1-
124 infected cells at different multiplicities of infection (MOI), in the absence and presence of WASA-1 (Fig.
125 2A). This revealed that WonAB provides robust protection against ICP1 at low MOI when only a subset
126 of cells is initially infected. In contrast, infection at high MOI, when most cells are simultaneously
127 infected, resulted in a growth arrest (Fig. 2A). This phenotype is characteristic of abortive infection,
128 wherein individual cell viability is sacrificed prior to the completion of phage replication to protect the
129 surrounding bacterial population[41]. Indeed, time-lapse microscopy showed that while both WT and

130 ΔWASA-1 cells swell upon infection, cells of the ΔWASA-1 go on to lyse within ~20min, whereas WT
131 cells remain in this swollen state without lysing for the 60min duration of the experiment (Fig. 2B,
132 Extended Data Fig. 6 and movie S1). Moreover, these growth-arrested cells persist in an intact state for
133 several hours before eventually undergoing lysis (Extended Data Fig. 7A-B). During this time ICP1-
134 infected cultures rebounded due to the growth of spontaneous O1-antigen mutants (Extended Data
135 Fig. 7C), which is the receptor for ICP1, as has been observed elsewhere[6]. Importantly, this is likely an
136 *in vitro* phenomenon since O1 antigen mutants are attenuated for virulence[42].

137 Efforts to isolate either a spontaneous or an evolved ICP1 escape mutant resistant to WonAB
138 have so far proved unsuccessful. Therefore, to study the mode of action of WonAB in more detail we
139 investigated different stages of the ICP1 lifecycle in the absence and presence of WASA-1[7,43]. First,
140 quantitative-PCR showed that ICP1 DNA replication proceeds similarly in both strain backgrounds,
141 albeit with a 2.7-fold defect in the WT background, indicating that WonAB neither restricts ICP1 DNA
142 on entry nor prevents the initiation of DNA replication (Fig. 2C). Second, microscopy revealed that
143 upon infection the nucleoids of both strains undergo dramatic changes in morphology by 4min post-
144 infection, with the nucleoid frequently appearing to contract along its long axis, likely representing the
145 action of ICP1-encoded nucleases and host-cell takeover[43,44] (Fig. 2D). Notably, whereas ΔWASA-1 cells
146 then rapidly went on to lyse, DNA in WT cells persisted in a highly compacted state and went on to
147 form toroidal structures, suggesting that WonAB does not act by simply degrading DNA. Third,
148 microscopy of ICP1-infected cells producing a fluorescent protein fusion to the ICP1 major capsid
149 protein revealed robust capsid assembly, lysis and release in the ΔWASA-1 background (Fig. 2E-G). In
150 contrast, capsid assembly was largely absent in WT cells (Fig. 2F). Taken together, these results show
151 that WonAB does not prevent the initial damage inflicted by ICP1, and suggest that WonAB is activated
152 after the initiation of ICP1 DNA replication and prevents progression to structural protein assembly.
153

154 **WonAB activation shuts down cell growth by inhibiting translation**

155 The data so far are consistent with WonAB aborting ICP1 infection via a lysis-independent mechanism
156 that targets the host cell. To test whether WonAB can be artificially activated in the absence of
157 infection, we overexpressed either the *wonAB* operon or each gene individually in an otherwise WT
158 background (Fig. 3A and Extended Data Fig. 8A). While *wonAB* and *wonA* had no apparent phenotype,
159 WonB overproduction was highly toxic, resulting in a growth arrest and a rapid loss in viability, with
160 >99% of cells non-viable within 30min (Fig. 3A-C and Extended Data Fig. 8A). Furthermore, toxicity was
161 dependent on WonB nuclease activity since the WonB[K71A] variant was non-toxic (Fig. 3B-C and
162 Extended Data Fig. 8A). One explanation for these data could be that WonAB is a toxin-antitoxin
163 system, with WonA acting as an antitoxin to neutralise the toxicity of WonB[45]. Indeed, the DarTG toxin-
164 antitoxin system has recently been shown to have activity against ICP1[46]. Arguing against this
165 hypothesis, however, WonB overproduction was not toxic in a Δ*wonAB* background, despite being
166 produced at similar levels to the control (Fig. 3A and Extended Data Fig. 8B-C). Moreover, deletion of
167 *wonA* or inactivation of WonA ATPase activity also abolished the toxicity associated with WonB
168 overproduction (Fig. 3A and Extended Data Fig. 8B-C). Thus, these results rule out a simple
169 sequestration mechanism and suggest that WonA is either required to activate WonB or that the two
170 proteins act together.

171 Microscopy revealed that following WonB overproduction growth-arrested cells exhibit
172 condensed nucleoids that at later stages display aberrant morphologies and are highly compacted (Fig.
173 3D and Extended Data Fig. 8D). Notably, the vast majority of cells retained DNA and purified genomic
174 DNA also remained intact (Extended Data Fig. 8D-E), indicating that toxicity does not result from
175 chromosomal DNA degradation. Since the nucleoid compaction phenotype resembled the effects of
176 antibiotics that inhibit translation[47], we investigated WonB production over time using Western
177 blotting (Fig. 3E). Remarkably, this revealed that compared to the inactivated WonB[K71A] control,
178 WonB is produced only for short time after induction, and by 30min post-induction was no longer
179 detectable. Importantly, qRT-PCR showed that *wonB* mRNA levels were induced similarly between the

180 two constructs and remained stable throughout the course of the experiment (Extended Data Fig. 8F).
181 These data suggested that (i) WonB overproduction inhibits translation and (ii) that WonB is likely
182 unstable. In agreement with these hypotheses, following inhibition of translation with
183 chloramphenicol, WonB rapidly disappeared in a Lon protease-dependent manner (Fig. 3F-G),
184 indicating that WonB is indeed unstable and subject to proteolytic degradation. Since in the absence
185 of ICP1, WonB was toxic only when produced in excess of WonA, Lon-mediated degradation likely
186 functions as a safety mechanism to reduce WonB accumulation and hence prevent auto-immunity.
187 Collectively, these results support a model whereby upon activation WonAB aborts phage infection by
188 inhibiting translation, and thus preventing the progression of the ICP1 lifecycle. Furthermore, since the
189 growth-arrest upon WonB overproduction does not result in genomic DNA degradation, these results
190 suggest that the target of WonB nuclease activity could be a rRNA or tRNA.
191
192 **VSP-II^{WASA} carries two distinct anti-phage defence systems**
193 The second genetic signature of the WASA lineage is a unique variant of VSP-II (Fig. 4A), wherein the
194 chemotaxis gene cluster from the prototypical VSP-II is replaced by a set of three novel genes
195 (A1552VC_00274-76) and a frame-shifted transposase gene[9,23,48]. Although these genes are not
196 predicted to be part of a known defence system, and lacked activity against ICP1-3, bioinformatic
197 analysis revealed that they encode proteins with domains characteristic of defence systems (see
198 below). Consistent with this, when this cluster was expressed in *E. coli* we observed anti-phage activity
199 against several major groups of the BASEL collection (Fig. 4B and Extended Data Fig. 9A). As outlined
200 below, genetic dissection revealed that this cluster encodes two independent systems, with the two-
201 gene operon VC_00274-75 encoding the GmrSD-like Type IV REase of WASA strains, GrwAB (Fig. 4C-E)
202 and VC_00276 encoding the *V. cholerae* Shedu, *Vc*SduA (Fig. 4F-H).
203 GrwAB showed potent anti-phage activity against all members of the *Queuovirinae* and
204 *Tevenvirinae* (*Straboviridae*), as well as some members of the *Markadamsvirinae* (*Demerecviridae*),
205 and both genes were required for protection (Fig. 4B). Interestingly, the signature feature of the
206 *Queuovirinae* and *Tevenvirinae* subfamilies is that their genomes contain hypermodified nucleobases

207 with either 7-deazaguanine modified guanosines or sugar-modified hydroxymethyl cytosines,
208 respectively, suggesting that GrwAB may recognise DNA modification[33,49,50]. In line with this
209 hypothesis, GrwAB resembles the GmrSD family of modification-dependent restriction enzymes, such
210 as GmrSD, BrxU and SspE[51-54] (Fig. 4C and Extended Data Fig. 10A-D). These are typically single protein
211 systems composed of an N-terminal DUF262 domain that functions as a DNA modification sensor, and
212 that uses NTP binding/hydrolysis to regulate the activity of a C-terminal His-Me nuclease domain
213 (DUF1524), which functions as an effector to target non-self DNA[51,53,55]. Indeed, GrwA is predicted to
214 share this architecture, with an N-terminal DUF262 domain containing the highly conserved QR,
215 DGQQR and FxxN motifs[51], coupled by an α-helical linker to a C-terminal DUF1524 domain containing
216 the canonical $\beta\beta\alpha$ fold and catalytic residues of the His-Me nuclease superfamily[56] (Fig. 4C and
217 Extended Data Fig. 10A-C). In contrast, and unlike known GmrSD systems, GrwB encoded by the second
218 gene contains an N-terminal DUF262 domain followed by multiple domains of unknown function (Fig.
219 4C and Extended Data Fig. 10D). Notably, variants designed to disrupt either the NTP hydrolysis of
220 DUF262 in GrwA[R81A] and GrwB[R86A], or the nuclease activity of DUF1524 in
221 GrwA[H431A]/[N521A/[N530A] all abolished anti-phage activity (Fig. 4D), indicating that GrwA and
222 GrwB function together.

223 Importantly, multiple independent escaper mutants of Bas24 were obtained that overcome
224 defence by GrwAB (Extended Data Fig. 11A). These escapers all contain changes in either the active
225 site or the DNA-binding surface of DpdA – the transglycosylase that inserts the 7-deazaguanine
226 modification into the DNA – consistent with the disruption of DNA modification leading to immune
227 evasion[57] (Extended Data Fig. 11B-D). Interestingly, growth kinetics of phage-infected cultures
228 producing GrwAB lacked the growth arrest or premature lysis typical of abortive infection (Fig. 4E).
229 However, cultures did go on to exhibit moderate-to-severe lysis, which microscopy revealed was due
230 to the presence of non-dividing filamentous cells (Extended Data Fig. 12 and movie S2), suggesting
231 that either GrwAB is unable to clear the infection prior to the cell sustaining irreversible damage or
232 that the cell is subject to collateral damage during phage defence. Finally, bioinformatic analyses

233 revealed that homologues of GrwAB are widespread and found in ~1% of genomes examined
234 (Extended Data Fig. 10E and table S4), suggesting that GrwAB represents a new member of an
235 emerging family of two-gene GmrSD-like modification-dependent restriction enzymes that includes
236 the recently discovered TgvAB system present in *V. cholerae* VPI-2[20,21]. Similar to TgvAB, the
237 requirement for both GrwA and GrwB suggests that these proteins likely act as a complex, which could
238 represent either a novel mode of action or else a mechanism to overcome phage-encoded anti-
239 defences. Notably, despite the similarities, GrwAB has an expanded range compared to TgvAB and is
240 also able to recognise 7-deazaguanine modified DNA. Furthermore, although GrwA, TgvB and GmrSD
241 all share a similar domain architecture, except for the shared N-terminal DUF262 domain GrwB and
242 TgvA are distinct from one another[20].

243 *Vc*SduA showed activity against all members of the T1-like *Drexlerviridae* family, with strong
244 protection against Bas1 (>10,000-fold), Bas03 and Bas08 (10-100-fold), while the remainder showed a
245 reduced plaque diameter that in the case of Bas03 and Bas05 was drastic (Fig. 4B and Extended Data
246 Fig. 9B). Sequence analysis and structural modelling showed that *Vc*SduA encodes an N-terminal GHKL
247 (Gyrase, Hsp90, Histidine Kinase, MutL) ATPase domain (HATPase_c) containing the highly conserved
248 motifs I-IV that define this ATPase superfamily[58,59], followed by a C-terminal PD-(D/E)xK nuclease
249 domain (DUF4263) that is also found in the Shedu defence system[15,60,61] (Fig. 4F and Extended Data
250 Fig. 13 A-C). Variants designed to disrupt either ATP hydrolysis *Vc*SduA[E27A] or nuclease activity
251 *Vc*SduA[K557A] both abolished anti-phage activity despite being produced at similar levels to WT
252 control (Fig. 4G and Extended Data Fig. 13D). Furthermore, growth kinetic experiments with phage-
253 infected cultures revealed similarly robust protection at all tested MOIs (Fig. 4H), consistent with
254 *Vc*SduA targeting and restricting the phage directly while preserving the viability of the host cell.

255 Modelling of *Vc*SduA as a dimer (Fig. 4F), which are typical for GHKL ATPases, confidently
256 predicted an entwined configuration with the GHKL ATPase domain sitting below a cavity formed by a
257 clamp-like middle domain, which in other GHKL family members mediates binding to DNA and protein
258 substrates[58,62]. Thus, these results suggest that the GHKL domain may act as a sensor to control the
259 activity of the C-terminal nuclease domain. Furthermore, bioinformatic analysis revealed that *Vc*SduA

260 homologues are widely distributed and present in ~1.2% of genomes examined (Extended Data Fig.
261 13E and table S5). Notably, GrwAB and *Vc*SduA were rarely found together outside of *V. cholerae* (table
262 S5), consistent with the demonstration above that they are independent systems. Interestingly,
263 proteins with a similar domain organisation to *Vc*SduA were previously annotated as paraMORC3, and
264 have recently been proposed to be part of the Shedu (SduA) defence system family due to the presence
265 of the signature Shedu domain DUF4263[59,60]. Indeed, both of these *in silico* predicted systems closely
266 resemble *Vc*SduA, suggesting that it is a newly identified member of the Shedu defence system family.
267

268 **Discussion**

269 The main discovery of this work is that the two unique genetic signatures (VSP-II^{WASA} and WASA-1) of
270 the WASA lineage encode three novel antiviral defence systems (GrwAB, *Vc*SduA and WonAB).
271 Previously, these elements have primarily been used as a molecular signature to track the origins of
272 these strains[9,23-25,63], but their significance for the success of the lineage and the Latin American
273 cholera epidemic has remained unknown. Here we demonstrate that combined these systems have
274 broad activity against diverse bacteriophage families and target two-thirds of the isolates in the BASEL
275 bacteriophage collection, including those with highly modified genomes. Importantly, we also show
276 that in the native *V. cholerae* host, the WonAB system carried on the WASA-1 prophage renders strains
277 resistant to ICP1 - the major predatory phage of pandemic *V. cholerae*[7]. Given the ongoing arms race
278 between *V. cholerae* and ICP1[10,13] and the established role of ICP1 predation in cholera epidemics[2,3,5,6],
279 it is therefore reasonable to assume that this would have provided a significant selective advantage
280 to the lineage. Nevertheless, since WonAB can also target other phages, then together with the
281 systems carried on VSP-II^{WASA}, this selective advantage may have been against phages other than ICP1.

282 Prior to the start of the epidemic in 1991, Latin America had been free from pandemic cholera
283 for almost 100 years[22,64]. However, following the introduction of the WASA lineage from West Africa
284 in the late 1980's, an explosive cholera epidemic spread rapidly throughout Latin America, with
285 >500,000 cases in Peru alone in 1991-92, and ongoing outbreaks continuing until 2001[9,22,25,26,64,65].
286 Given our findings we therefore propose that the combined activities of the defence systems encoded

287 on VSP-II^{WASA} and WASA-1 are responsible for the success of the WASA lineage and envisage at least
288 two possible scenarios by which this could have occurred. Firstly, the acquisition of these systems in
289 Africa could have allowed the strains to resist local *vibrio*phages, triggering the proliferation of the
290 lineage that therefore facilitated the transfer to South America. Notably, cholera outbreaks were
291 ongoing in Western and Central Africa just prior to the start of the Latin American epidemic, and
292 intensified in the years afterwards[25,26]. Furthermore, strains containing VSP-II^{WASA} and WASA-1
293 continued to circulate in Western/Central Africa up until the late 1990's, including in the strains
294 responsible for the 1987-1996 Angolan cholera epidemic[25,26,66]. Secondly, the defences provided by
295 these elements could have played a more direct role in the transmission, for example by allowing the
296 WASA lineage to overcome an entry barrier posed by phages associated with local non-pandemic *V.*
297 *cholerae* strains endemic to South America that might have prevented previous introductions. In
298 support of these proposals, the ability to defend against phage predation is thought to play a key role
299 in the observed evolution of local *V. cholerae* lineages, which then go on to be successful before
300 subsequently being replaced[10,13]. Finally, while further work will be necessary to decipher the
301 mechanistic details of the newly discovered defence systems, this work provides new insights into the
302 evolution of one of the major epidemic lineages of the seventh cholera pandemic. Moreover, while
303 7PET strains are typically considered to be clonal based on the phylogeny of the core genome, these
304 results reinforce the need to consider the role of the accessory genomes in the success of novel
305 lineages and therefore understanding their pandemic potential.
306

307 **References**

308 1 Georjon, H. & Bernheim, A. The highly diverse antiphage defence systems of bacteria. *Nat Rev*
309 *Microbiol* **21**, 686-700, doi:10.1038/s41579-023-00934-x (2023).
310 2 Faruque, S. M. *et al.* Seasonal epidemics of cholera inversely correlate with the prevalence of
311 environmental cholera phages. *Proc Natl Acad Sci U S A* **102**, 1702-7,
312 doi:10.1073/pnas.0408992102 (2005).
313 3 Faruque, S. M. *et al.* Self-limiting nature of seasonal cholera epidemics: Role of host-mediated
314 amplification of phage. *Proc Natl Acad Sci U S A* **102**, 6119-24, doi:10.1073/pnas.0502069102
315 (2005).
316 4 Jensen, M. A., Faruque, S. M., Mekalanos, J. J. & Levin, B. R. Modeling the role of bacteriophage
317 in the control of cholera outbreaks. *Proc Natl Acad Sci U S A* **103**, 4652-7,
318 doi:10.1073/pnas.0600166103 (2006).

319 5 Madi, N. *et al.* Phage predation, disease severity, and pathogen genetic diversity in cholera
320 patients. *Science* **384**, eadj3166, doi:10.1126/science.adj3166 (2024).
321 6 Seed, K. D. *et al.* Evidence of a dominant lineage of *Vibrio cholerae*-specific lytic
322 bacteriophages shed by cholera patients over a 10-year period in Dhaka, Bangladesh. *mBio* **2**,
323 e00334-10, doi:10.1128/mBio.00334-10 (2011).
324 7 Boyd, C. M. *et al.* Bacteriophage ICP1: A Persistent Predator of *Vibrio cholerae*. *Annu Rev Virol*
325 **8**, 285-304, doi:10.1146/annurev-virology-091919-072020 (2021).
326 8 Yen, M., Cairns, L. S. & Camilli, A. A cocktail of three virulent bacteriophages prevents *Vibrio*
327 *cholerae* infection in animal models. *Nat Commun* **8**, 14187, doi:10.1038/ncomms14187
328 (2017).
329 9 Mutreja, A. *et al.* Evidence for several waves of global transmission in the seventh cholera
330 pandemic. *Nature* **477**, 462-5, doi:10.1038/nature10392 (2011).
331 10 LeGault, K. N. *et al.* Temporal shifts in antibiotic resistance elements govern phage-pathogen
332 conflicts. *Science* **373**, doi:10.1126/science.abg2166 (2021).
333 11 Seed, K. D., Lazinski, D. W., Calderwood, S. B. & Camilli, A. A bacteriophage encodes its own
334 CRISPR/Cas adaptive response to evade host innate immunity. *Nature* **494**, 489-91,
335 doi:10.1038/nature11927 (2013).
336 12 O'Hara, B. J., Barth, Z. K., McKitterick, A. C. & Seed, K. D. A highly specific phage defense system
337 is a conserved feature of the *Vibrio cholerae* mobilome. *PLoS Genet* **13**, e1006838,
338 doi:10.1371/journal.pgen.1006838 (2017).
339 13 Angermeyer, A. *et al.* Evolutionary Sweeps of Subviral Parasites and Their Phage Host Bring
340 Unique Parasite Variants and Disappearance of a Phage CRISPR-Cas System. *mBio* **13**,
341 e0308821, doi:10.1128/mbio.03088-21 (2021).
342 14 Davies, B. W., Bogard, R. W., Young, T. S. & Mekalanos, J. J. Coordinated regulation of
343 accessory genetic elements produces cyclic di-nucleotides for *V. cholerae* virulence. *Cell* **149**,
344 358-70, doi:10.1016/j.cell.2012.01.053 (2012).
345 15 Doron, S. *et al.* Systematic discovery of antiphage defense systems in the microbial
346 pangenome. *Science* **359**, doi:10.1126/science.aar4120 (2018).
347 16 Severin, G. B. *et al.* Direct activation of a phospholipase by cyclic GMP-AMP in El Tor *Vibrio*
348 *cholerae*. *Proc Natl Acad Sci U S A* **115**, E6048-E55, doi:10.1073/pnas.1801233115 (2018).
349 17 Cohen, D. *et al.* Cyclic GMP-AMP signalling protects bacteria against viral infection. *Nature*
350 **574**, 691-95, doi:10.1038/s41586-019-1605-5 (2019).
351 18 Hsueh, B. Y. *et al.* Phage defence by deaminase-mediated depletion of deoxynucleotides in
352 bacteria. *Nat Microbiol* **7**, 1210-20, doi:10.1038/s41564-022-01162-4 (2022).
353 19 Jaskólska, M., Adams, D. W. & Blokesch, M. Two defence systems eliminate plasmids from
354 seventh pandemic *Vibrio cholerae*. *Nature* **604**, 323-29, doi:10.1038/s41586-022-04546-y
355 (2022).
356 20 Vizzarro, G., Lemopoulos, A., Adams, D. W. & Blokesch, M. *Vibrio cholerae* pathogenicity island
357 2 encodes two distinct types of restriction systems. *J Bacteriol*, e0014524,
358 doi:10.1128/jb.00145-24 (2024).
359 21 Gomez, J. B. & Waters, C. M. A *Vibrio cholerae* Type IV restriction system targets glucosylated
360 5-hydroxymethylcytosine to protect against phage infection. *J Bacteriol*, e0014324,
361 doi:10.1128/jb.00143-24 (2024).
362 22 Kumate, J., Sepúlveda, J. & Gutiérrez, G. Cholera epidemiology in Latin America and
363 perspectives for eradication. *Bulletin de l'Institut Pasteur* **96**, 217-26,
364 doi:https://doi.org/10.1016/S0020-2452(99)80002-5 (1998).
365 23 Nusrin, S. *et al.* Peruvian *Vibrio cholerae* O1 El Tor strains possess a distinct region in the *Vibrio*
366 seventh pandemic island-II that differentiates them from the prototype seventh pandemic El
367 Tor strains. *J Med Microbiol* **58**, 342-54, doi:10.1099/jmm.0.005397-0 (2009).
368 24 Garza, D. R. *et al.* Genome-wide study of the defective sucrose fermenter strain of *Vibrio*
369 *cholerae* from the Latin American cholera epidemic. *PLoS One* **7**, e37283,
370 doi:10.1371/journal.pone.0037283 (2012).

371 25 Domman, D. *et al.* Integrated view of *Vibrio cholerae* in the Americas. *Science* **358**, 789-93,
372 doi:10.1126/science.aao2136 (2017).
373 26 Weill, F. X. *et al.* Genomic history of the seventh pandemic of cholera in Africa. *Science* **358**,
374 785-89, doi:10.1126/science.aad5901 (2017).
375 27 Lemos Rocha, L. F. *et al.* The VarA-CsrA regulatory pathway influences cell shape in *Vibrio*
376 *cholerae*. *PLoS Genet* **18**, e1010143, doi:10.1371/journal.pgen.1010143 (2022).
377 28 Rousset, F. *et al.* Phages and their satellites encode hotspots of antiviral systems. *Cell Host*
378 *Microbe* **30**, 740-53 e5, doi:10.1016/j.chom.2022.02.018 (2022).
379 29 Vassallo, C. N., Doering, C. R., Littlehale, M. L., Teodoro, G. I. C. & Laub, M. T. A functional
380 selection reveals previously undetected anti-phage defence systems in the E. coli pangenome.
381 *Nat Microbiol* **7**, 1568-79, doi:10.1038/s41564-022-01219-4 (2022).
382 30 Patel, P. H. & Maxwell, K. L. Prophages provide a rich source of antiphage defense systems.
383 *Curr Opin Microbiol* **73**, 102321, doi:10.1016/j.mib.2023.102321 (2023).
384 31 Krishnan, A., Burroughs, A. M., Iyer, L. M. & Aravind, L. Comprehensive classification of ABC
385 ATPases and their functional radiation in nucleoprotein dynamics and biological conflict
386 systems. *Nucleic Acids Res* **48**, 10045-75, doi:10.1093/nar/gkaa726 (2020).
387 32 Steczkiewicz, K., Muszewska, A., Knizewski, L., Rychlewski, L. & Ginalski, K. Sequence, structure
388 and functional diversity of PD-(D/E)XK phosphodiesterase superfamily. *Nucleic Acids Res* **40**,
389 7016-45, doi:10.1093/nar/gks382 (2012).
390 33 Maffei, E. *et al.* Systematic exploration of *Escherichia coli* phage-host interactions with the
391 BASEL phage collection. *PLoS Biol* **19**, e3001424, doi:10.1371/journal.pbio.3001424 (2021).
392 34 Schiltz, C. J., Adams, M. C. & Chappie, J. S. The full-length structure of *Thermus scotoductus*
393 OLD defines the ATP hydrolysis properties and catalytic mechanism of Class 1 OLD family
394 nucleases. *Nucleic Acids Res* **48**, 2762-76, doi:10.1093/nar/gkaa059 (2020).
395 35 Antine, S. P. *et al.* Structural basis of Gabija anti-phage defence and viral immune evasion.
396 *Nature* **625**, 360-65, doi:10.1038/s41586-023-06855-2 (2024).
397 36 Burman, N. *et al.* A virally-encoded tRNA neutralizes the PARIS antiviral defence system.
398 *Nature*, doi:10.1038/s41586-024-07874-3 (2024).
399 37 Deep, A., Liang, Q., Enustun, E., Pogliano, J. & Corbett, K. D. Architecture and activation
400 mechanism of the bacterial PARIS defence system. *Nature*, doi:10.1038/s41586-024-07772-8
401 (2024).
402 38 Li, Y. *et al.* PtuA and PtuB assemble into an inflammasome-like oligomer for anti-phage
403 defense. *Nat Struct Mol Biol* **31**, 413-23, doi:10.1038/s41594-023-01172-8 (2024).
404 39 Dot, E. W., Thomason, L. C. & Chappie, J. S. Everything OLD is new again: How structural,
405 functional, and bioinformatic advances have redefined a neglected nuclease family. *Mol*
406 *Microbiol* **120**, 122-40, doi:10.1111/mmi.15074 (2023).
407 40 Payne, L. J., Hughes, T. C. D., Fineran, P. C. & Jackson, S. A. New antiviral defences are
408 genetically embedded within prokaryotic immune systems. *bioRxiv*, 2024.01.29.577857,
409 doi:10.1101/2024.01.29.577857 (2024).
410 41 Rousset, F. & Sorek, R. The evolutionary success of regulated cell death in bacterial immunity.
411 *Curr Opin Microbiol* **74**, 102312, doi:10.1016/j.mib.2023.102312 (2023).
412 42 Seed, K. D. *et al.* Phase variable O antigen biosynthetic genes control expression of the major
413 protective antigen and bacteriophage receptor in *Vibrio cholerae* O1. *PLoS Pathog* **8**,
414 e1002917, doi:10.1371/journal.ppat.1002917 (2012).
415 43 Barth, Z. K., Netter, Z., Angermeyer, A., Bhardwaj, P. & Seed, K. D. A Family of Viral Satellites
416 Manipulates Invading Virus Gene Expression and Can Affect Cholera Toxin Mobilization.
417 *mSystems* **5**, doi:10.1128/mSystems.00358-20 (2020).
418 44 McKitterick, A. C., Hays, S. G., Johura, F. T., Alam, M. & Seed, K. D. Viral Satellites Exploit Phage
419 Proteins to Escape Degradation of the Bacterial Host Chromosome. *Cell Host Microbe* **26**, 504-
420 14 e4, doi:10.1016/j.chom.2019.09.006 (2019).
421 45 Jurėnas, D., Fraikin, N., Goormaghtigh, F. & Van Melderen, L. Biology and evolution of bacterial
422 toxin-antitoxin systems. *Nat Rev Microbiol* **20**, 335-50, doi:10.1038/s41579-021-00661-1
423 (2022).

46 Patel, K. M. & Seed, K. D. Sporadic phage defense in epidemic *Vibrio cholerae* mediated by the toxin-antitoxin system DarTG is countered by a phage-encoded antitoxin mimic. *bioRxiv*, doi:10.1101/2023.12.14.571748 (2023).

47 Nonejuie, P., Burkart, M., Pogliano, K. & Pogliano, J. Bacterial cytological profiling rapidly identifies the cellular pathways targeted by antibacterial molecules. *Proc Natl Acad Sci U S A* **110**, 16169-74, doi:10.1073/pnas.1311066110 (2013).

48 Murphy, S. G., Johnson, B. A., Ledoux, C. M. & Dörr, T. *Vibrio cholerae*'s mysterious Seventh Pandemic island (VSP-II) encodes novel Zur-regulated zinc starvation genes involved in chemotaxis and cell congregation. *PLoS Genet* **17**, e1009624, doi:10.1371/journal.pgen.1009624 (2021).

49 Hutinet, G. *et al.* 7-Deazaguanine modifications protect phage DNA from host restriction systems. *Nat Commun* **10**, 5442, doi:10.1038/s41467-019-13384-y (2019).

50 Hutinet, G., Lee, Y. J., de Crécy-Lagard, V. & Weigele, P. R. Hypermodified DNA in Viruses of *E. coli* and *Salmonella*. *EcoSal Plus* **9**, eESP00282019, doi:10.1128/ecosalplus.ESP-0028-2019 (2021).

51 Machnicka, M. A., Kaminska, K. H., Dunin-Horkawicz, S. & Bujnicki, J. M. Phylogenomics and sequence-structure-function relationships in the GmrSD family of Type IV restriction enzymes. *BMC Bioinformatics* **16**, 336, doi:10.1186/s12859-015-0773-z (2015).

52 He, X. *et al.* Expression and purification of a single-chain Type IV restriction enzyme Eco94GmrSD and determination of its substrate preference. *Sci Rep* **5**, 9747, doi:10.1038/srep09747 (2015).

53 Picton, D. M. *et al.* The phage defence island of a multidrug resistant plasmid uses both BREX and type IV restriction for complementary protection from viruses. *Nucleic Acids Res* **49**, 11257-73, doi:10.1093/nar/gkab906 (2021).

54 Xiong, X. *et al.* SspABCD-SspE is a phosphorothioation-sensing bacterial defence system with broad anti-phage activities. *Nat Microbiol* **5**, 917-28, doi:10.1038/s41564-020-0700-6 (2020).

55 Gao, H. *et al.* Nicking mechanism underlying the DNA phosphorothioate-sensing antiphage defense by SspE. *Nat Commun* **13**, 6773, doi:10.1038/s41467-022-34505-0 (2022).

56 Jablonska, J., Matelska, D., Steczkiewicz, K. & Ginalski, K. Systematic classification of the His-Me finger superfamily. *Nucleic Acids Res* **45**, 11479-94, doi:10.1093/nar/gkx924 (2017).

57 Gedara, S. H. *et al.* 7-Deazaguanines in DNA: functional and structural elucidation of a DNA modification system. *Nucleic Acids Res* **51**, 3836-54, doi:10.1093/nar/gkad141 (2023).

58 Dutta, R. & Inouye, M. GHKL, an emergent ATPase/kinase superfamily. *Trends Biochem Sci* **25**, 24-8, doi:10.1016/s0968-0004(99)01503-0 (2000).

59 Iyer, L. M., Abhiman, S. & Aravind, L. MutL homologs in restriction-modification systems and the origin of eukaryotic MORC ATPases. *Biol Direct* **3**, 8, doi:10.1186/1745-6150-3-8 (2008).

60 Gu, Y. *et al.* Bacterial Shedu immune nucleases share a common enzymatic core regulated by diverse sensor domains. *bioRxiv*, 2023.08.10.552793, doi:10.1101/2023.08.10.552793 (2023).

61 Loeff, L., Walter, A., Rosalen, G. T. & Jinek, M. DNA end sensing and cleavage by the Shedu anti-phage defense system. *bioRxiv*, 2023.08.10.552762, doi:10.1101/2023.08.10.552762 (2023).

62 Corbett, K. D. & Berger, J. M. Structural dissection of ATP turnover in the prototypical GHL ATPase TopoVI. *Structure* **13**, 873-82, doi:10.1016/j.str.2005.03.013 (2005).

63 Morais, L. L. *et al.* Population and genetic study of *Vibrio cholerae* from the amazon environment confirms that the WASA-1 prophage is the main marker of the epidemic strain that circulated in the region. *PLoS One* **8**, e81372, doi:10.1371/journal.pone.0081372 (2013).

64 Tauxe, R. V., Mintz, E. D. & Quick, R. E. Epidemic cholera in the new world: translating field epidemiology into new prevention strategies. *Emerg Infect Dis* **1**, 141-6, doi:10.3201/eid0104.950408 (1995).

65 Dorman, M. J. *et al.* Genomics of the Argentinian cholera epidemic elucidate the contrasting dynamics of epidemic and endemic *Vibrio cholerae*. *Nat Commun* **11**, 4918, doi:10.1038/s41467-020-18647-7 (2020).

66 Valia, R. *et al.* *Vibrio cholerae* O1 epidemic variants in Angola: a retrospective study between 1992 and 2006. *Front Microbiol* **4**, 354, doi:10.3389/fmicb.2013.00354 (2013).
67 Lim, A. N. W., Yen, M., Seed, K. D., Lazinski, D. W. & Camilli, A. A Tail Fiber Protein and a Receptor-Binding Protein Mediate ICP2 Bacteriophage Interactions with *Vibrio cholerae* OmpU. *J Bacteriol* **203**, e0014121, doi:10.1128/JB.00141-21 (2021).
68 Eberhart-Phillips, J. *et al.* An outbreak of cholera from food served on an international aircraft. *Epidemiol Infect* **116**, 9-13, doi:10.1017/s0950268800058891 (1996).
69 Yildiz, F. H. & Schoolnik, G. K. Role of *rpoS* in stress survival and virulence of *Vibrio cholerae*. *J Bacteriol* **180**, 773-84, doi:10.1128/JB.180.4.773-784.1998 (1998).
70 Matthey, N., Drebes Dörr, N. C. & Blokesch, M. Long-Read-Based Genome Sequences of Pandemic and Environmental *Vibrio cholerae* Strains. *Microbiol Resour Announc* **7**, doi:10.1128/MRA.01574-18 (2018).
71 Aoki, S. K. *et al.* A universal biomolecular integral feedback controller for robust perfect adaptation. *Nature* **570**, 533-37, doi:10.1038/s41586-019-1321-1 (2019).
72 Simon, R., Priefer, U. & Pühler, A. A Broad Host Range Mobilization System for In Vivo Genetic Engineering: Transposon Mutagenesis in Gram Negative Bacteria. *Bio/Technology* **1**, 784-91, doi:10.1038/nbt1183-784 (1983).
73 Ferrières, L. *et al.* Silent mischief: bacteriophage Mu insertions contaminate products of *Escherichia coli* random mutagenesis performed using suicidal transposon delivery plasmids mobilized by broad-host-range RP4 conjugative machinery. *J Bacteriol* **192**, 6418-27, doi:10.1128/JB.00621-10 (2010).
74 Marvig, R. L. & Blokesch, M. Natural transformation of *Vibrio cholerae* as a tool--optimizing the procedure. *BMC Microbiol* **10**, 155, doi:10.1186/1471-2180-10-155 (2010).
75 De Souza Silva, O. & Blokesch, M. Genetic manipulation of *Vibrio cholerae* by combining natural transformation with FLP recombination. *Plasmid* **64**, 186-95, doi:10.1016/j.plasmid.2010.08.001 (2010).
76 Blokesch, M. TransFLP-a method to genetically modify *Vibrio cholerae* based on natural transformation and FLP-recombination. *J Vis Exp*, doi:10.3791/3761 (2012).
77 Meibom, K. L. *et al.* The *Vibrio cholerae* chitin utilization program. *Proc Natl Acad Sci U S A* **101**, 2524-9, doi:10.1073/pnas.0308707101 (2004).
78 Bao, Y., Lies, D. P., Fu, H. & Roberts, G. P. An improved Tn7-based system for the single-copy insertion of cloned genes into chromosomes of gram-negative bacteria. *Gene* **109**, 167-8, doi:10.1016/0378-1119(91)90604-a (1991).
79 Ducret, A., Quardokus, E. M. & Brun, Y. V. MicrobeJ, a tool for high throughput bacterial cell detection and quantitative analysis. *Nat Microbiol* **1**, 16077, doi:10.1038/nmicrobiol.2016.77 (2016).
80 Lo Scrudato, M. & Blokesch, M. The regulatory network of natural competence and transformation of *Vibrio cholerae*. *PLoS Genet* **8**, e1002778, doi:10.1371/journal.pgen.1002778 (2012).
81 Tesson, F. *et al.* Systematic and quantitative view of the antiviral arsenal of prokaryotes. *Nat Commun* **13**, 2561, doi:10.1038/s41467-022-30269-9 (2022).
82 Payne, L. J. *et al.* PADLOC: a web server for the identification of antiviral defence systems in microbial genomes. *Nucleic Acids Res* **50**, W541-W50, doi:10.1093/nar/gkac400 (2022).
83 Zimmermann, L. *et al.* A Completely Reimplemented MPI Bioinformatics Toolkit with a New HHpred Server at its Core. *J Mol Biol* **430**, 2237-43, doi:10.1016/j.jmb.2017.12.007 (2018).
84 Holm, L., Laiho, A., Törönen, P. & Salgado, M. DALI shines a light on remote homologs: One hundred discoveries. *Protein Sci* **32**, e4519, doi:10.1002/pro.4519 (2023).
85 Abramson, J. *et al.* Accurate structure prediction of biomolecular interactions with AlphaFold 3. *Nature* **630**, 493-500, doi:10.1038/s41586-024-07487-w (2024).
86 Crooks, G. E., Hon, G., Chandonia, J. M. & Brenner, S. E. WebLogo: a sequence logo generator. *Genome Res* **14**, 1188-90, doi:10.1101/gr.849004 (2004).

527 87 Katoh, K. & Standley, D. M. MAFFT multiple sequence alignment software version 7:
528 improvements in performance and usability. *Mol Biol Evol* **30**, 772-80,
529 doi:10.1093/molbev/mst010 (2013).
530 88 Gilchrist, C. L. M. & Chooi, Y. H. clinker & clustermap.js: automatic generation of gene cluster
531 comparison figures. *Bioinformatics* **37**, 2473-75, doi:10.1093/bioinformatics/btab007 (2021).
532 89 Abby, S. S., Néron, B., Ménager, H., Touchon, M. & Rocha, E. P. MacSyFinder: a program to
533 mine genomes for molecular systems with an application to CRISPR-Cas systems. *PLoS One* **9**,
534 e110726, doi:10.1371/journal.pone.0110726 (2014).
535 90 Eddy, S. R. Accelerated Profile HMM Searches. *PLoS Comput Biol* **7**, e1002195,
536 doi:10.1371/journal.pcbi.1002195 (2011).
537 91 Stokar-Avihail, A. *et al.* Discovery of phage determinants that confer sensitivity to bacterial
538 immune systems. *Cell* **186**, 1863-76 e16, doi:10.1016/j.cell.2023.02.029 (2023).
539 92 Wick, R. R., Judd, L. M., Gorrie, C. L. & Holt, K. E. Unicycler: Resolving bacterial genome
540 assemblies from short and long sequencing reads. *PLoS Comput Biol* **13**, e1005595,
541 doi:10.1371/journal.pcbi.1005595 (2017).
542 93 Durbin, R., De Sanctis, B. & Blumer, M. Rotate: A command-line program to rotate circular
543 DNA sequences to start at a given position or string. *Wellcome Open Res* **8**, 401,
544 doi:10.12688/wellcomeopenres.19568.1 (2023).
545 94 Page, A. J. *et al.* SNP-sites: rapid efficient extraction of SNPs from multi-FASTA alignments.
546 *Microb Genom* **2**, e000056, doi:10.1099/mgen.0.000056 (2016).
547 95 Chattopadhyay, D. J. *et al.* New phage typing scheme for *Vibrio cholerae* O1 biotype El Tor
548 strains. *J Clin Microbiol* **31**, 1579-85, doi:10.1128/jcm.31.6.1579-1585.1993 (1993).
549 96 Drebes Dörr, N. C., Lemopoulos, A. & Blokesch, M. Exploring Mobile Genetic Elements in *Vibrio*
550 *cholerae*. *bioRxiv*, 2024.07.25.605194, doi:10.1101/2024.07.25.605194 (2024).
551 97 Heidelberg, J. F. *et al.* DNA sequence of both chromosomes of the cholera pathogen *Vibrio*
552 *cholerae*. *Nature* **406**, 477-83, doi:10.1038/35020000 (2000).
553 98 Pearson, G. D., Woods, A., Chiang, S. L. & Mekalanos, J. J. CTX genetic element encodes a site-
554 specific recombination system and an intestinal colonization factor. *Proc Natl Acad Sci U S A*
555 **90**, 3750-4, doi:10.1073/pnas.90.8.3750 (1993).
556 99 Stutzmann, S. & Blokesch, M. Comparison of chitin-induced natural transformation in
557 pandemic *Vibrio cholerae* O1 El Tor strains. *Environ Microbiol* **22**, 4149-66, doi:10.1111/1462-
558 2920.15214 (2020).
559 100 Miller, V. L., DiRita, V. J. & Mekalanos, J. J. Identification of *toxS*, a regulatory gene whose
560 product enhances *toxR*-mediated activation of the cholera toxin promoter. *J Bacteriol* **171**,
561 1288-93, doi:10.1128/jb.171.3.1288-1293.1989 (1989).
562 101 Wachsmuth, I. K. *et al.* The molecular epidemiology of cholera in Latin America. *J Infect Dis*
563 **167**, 621-6, doi:10.1093/infdis/167.3.621 (1993).
564 102 Blokesch, M. & Schoolnik, G. K. Serogroup conversion of *Vibrio cholerae* in aquatic reservoirs.
565 *PLoS Pathog* **3**, e81, doi:10.1371/journal.ppat.0030081 (2007).
566 103 Metzger, L. C. *et al.* Independent Regulation of Type VI Secretion in *Vibrio cholerae* by TfoX
567 and TfoY. *Cell Rep* **15**, 951-58, doi:10.1016/j.celrep.2016.03.092 (2016).
568 104 Adams, D. W., Stutzmann, S., Stoudmann, C. & Blokesch, M. DNA-uptake pili of *Vibrio cholerae*
569 are required for chitin colonization and capable of kin recognition via sequence-specific self-
570 interaction. *Nat Microbiol* **4**, 1545-57, doi:10.1038/s41564-019-0479-5 (2019).
571 105 Angermeyer, A., Das, M. M., Singh, D. V. & Seed, K. D. Analysis of 19 Highly Conserved *Vibrio*
572 *cholerae* Bacteriophages Isolated from Environmental and Patient Sources Over a Twelve-Year
573 Period. *Viruses* **10**, doi:10.3390/v10060299 (2018).
574 106 Seed, K. D. *et al.* Evolutionary consequences of intra-patient phage predation on microbial
575 populations. *Elife* **3**, e03497, doi:10.7554/eLife.03497 (2014).
576 107 O'Hara, B. J., Alam, M. & Ng, W. L. The *Vibrio cholerae* Seventh Pandemic Islands act in tandem
577 to defend against a circulating phage. *PLoS Genet* **18**, e1010250,
578 doi:10.1371/journal.pgen.1010250 (2022).
579

Acknowledgments

We thank all the members of the Blokesch laboratory for constructive feedback throughout the project. We also gratefully acknowledge K. D. Seed (University of California, Berkeley) and W.-L. Ng (Tufts University School of Medicine, Boston) for the gift of ICP phages, and A. Harms (ETH, Zürich) for the gift of the BASEL collection.

Funding

European Research Council Consolidator Grant 724630 (MB)

Swiss National Research Foundation 310030_185022 (MB)

HHMI International Scholarship 55008726 (MB)

EPFL intramural funding (MB)

Author contributions

Conceptualization: DWA, MJ and MB

Methodology: DWA, MJ, AL, and MB

Investigation: DWA, MJ, AL, SS, LR, LB and MB

Visualization: DWA

Funding acquisition: MB

Supervision: DWA and MB

Writing – original draft: DWA

Writing – review & editing: DWA, MJ and MB

Competing interests

Authors declare that they have no competing interests.

Data availability

All data are available in the main text or the supplementary materials.

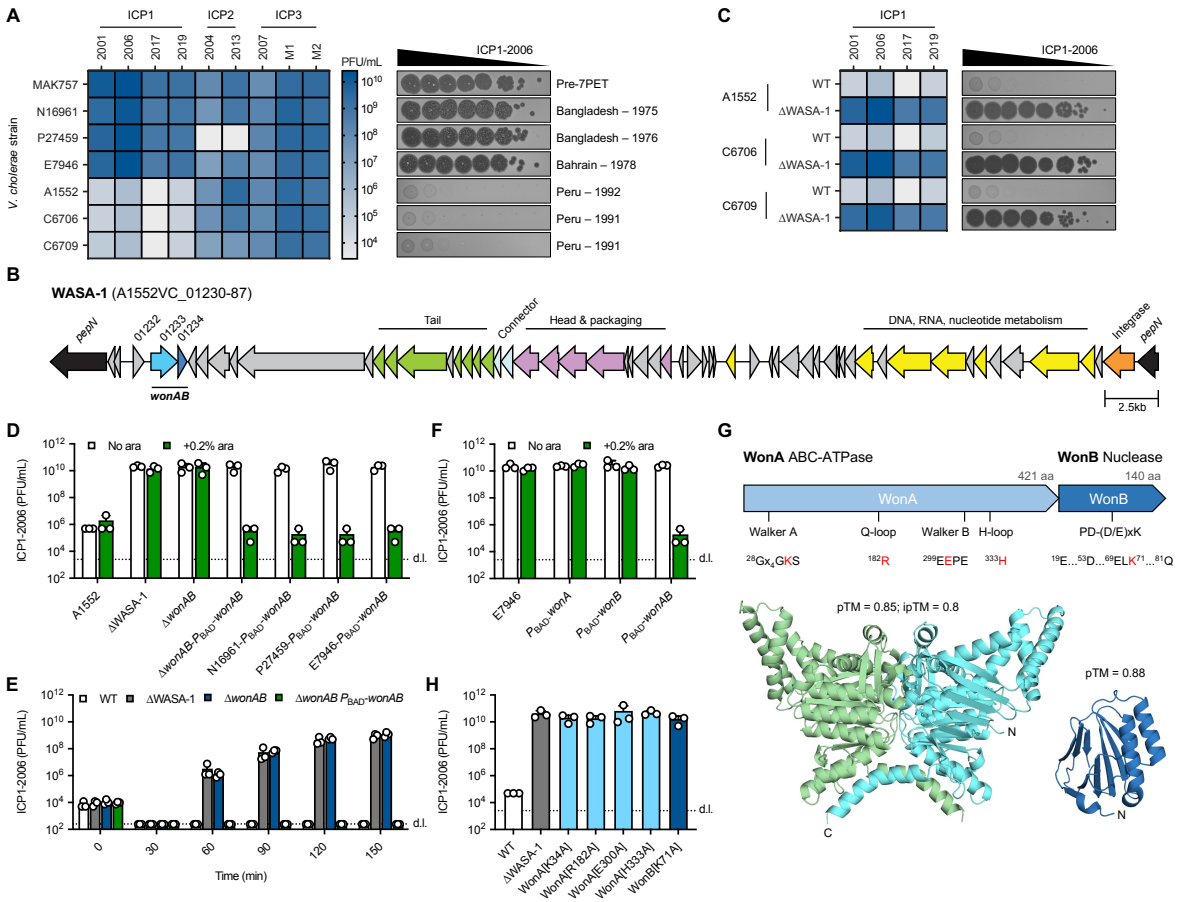

Fig. 1. WonAB carried on WASA-1 prophage renders WASA lineage ICP1 resistant. (**A**) Heat-map showing mean plaque-forming units (PFU/mL) of diverse ICP1-3 isolates determined by plaque assays on wave 1 *V. cholerae* strains, as compared to a pre-7th pandemic control (MAK757), shown alongside 10-fold serial dilution plaque assays of ICP1-2006. Data represent the results of three independent repeats. Strain P27459 encodes a naturally occurring resistant variant of the ICP2 receptor OmpU[67]. (**B**) Schematic of the WASA-1 prophage highlighting *wonAB* and genes with predicted functions in prophage biology. (**C**) Heat-map showing mean PFU/mL of diverse ICP1 isolates determined by plaque assays on Peruvian *V. cholerae* strains in WT and ΔWASA-1 backgrounds, determined as in (**A**). (**D**) Plaque assay showing the effects of ΔWASA-1, Δ*wonAB* and *wonAB* complementation in strain A1552 on ICP1-2006 PFU/mL alongside the effect of producing WonAB in non-WASA strains. (**E**) Replication assay showing change in PFU/mL over time following infection of the indicated A1552 cultures with *c.a.* 10^3-10^4 PFU of ICP1-2006. (**F**) Plaque assay showing effect of E7946 derivatives producing either WonA, WonB or WonAB on ICP1-2006 PFU/mL. Where indicated, strains in (**D**-**F**) contain a chromosomally integrated transposon carrying the arabinose-inducible P_{BAD}- promoter, induced by the addition of 0.2% arabinose. (**G**) Predicted structures of the WonA dimer and WonB generated using AlphaFold3 shown below schematic (top) indicating the conserved motifs. Residues targeted by site-directed mutagenesis are highlighted in red. (**H**) Plaque assay testing the effect of WonA and WonB site-directed variants expressed from their native locus on ICP1-2006 PFU/mL. Bar charts show the mean + s.d. from 3 independent repeats. d.l. = detection limit.

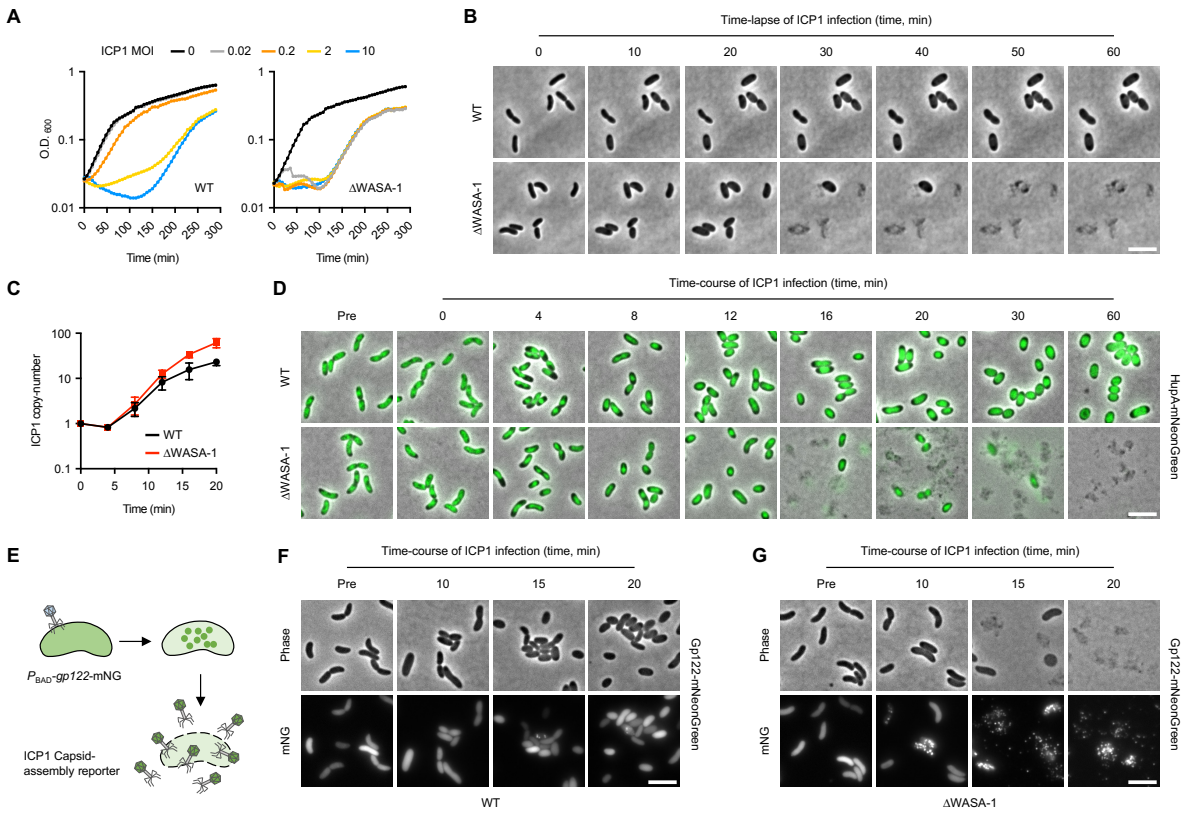

Fig. 2. WonAB protects cells by lysis-independent abortive infection. (**A**) Growth kinetics of *V. cholerae* strain A1552 in the presence (WT) and absence of WASA-1 (ΔWASA-1), with either no phage or infected at time 0 with ICP1-2006 at the indicated MOI. Data are representative of three independent repeats. (**B**) Time-lapse microscopy comparing exponentially growing cells of *V. cholerae* A1552 WT and ΔWASA-1 strains after infection with ICP1-2006 at MOI 5. (**C**) Fold-change in ICP1-2006 genome copy number relative to time 0, as determined by qPCR, after infection of either WT or ΔWASA-1 strains with ICP1-2006 at MOI 0.1. (**D**) Time-course microscopy snapshots comparing cell morphology and cellular DNA content, as monitored by a HupA-mNeonGreen fusion, in WT and ΔWASA-1 backgrounds following infection with ICP1-2006 at MOI 5. (**E-G**) Time-course microscopy snapshots comparing ICP1 capsid assembly, as monitored by the incorporation of a host-cell produced mNeonGreen (mNG) fusion to the ICP1 major capsid protein Gp122 (**E**), in either WT (**F**) or ΔWASA-1 (**G**) backgrounds, following infection with ICP1-2006 at MOI 5. All images are representative of the results of three independent experiments. Scale bars = 5 µm.

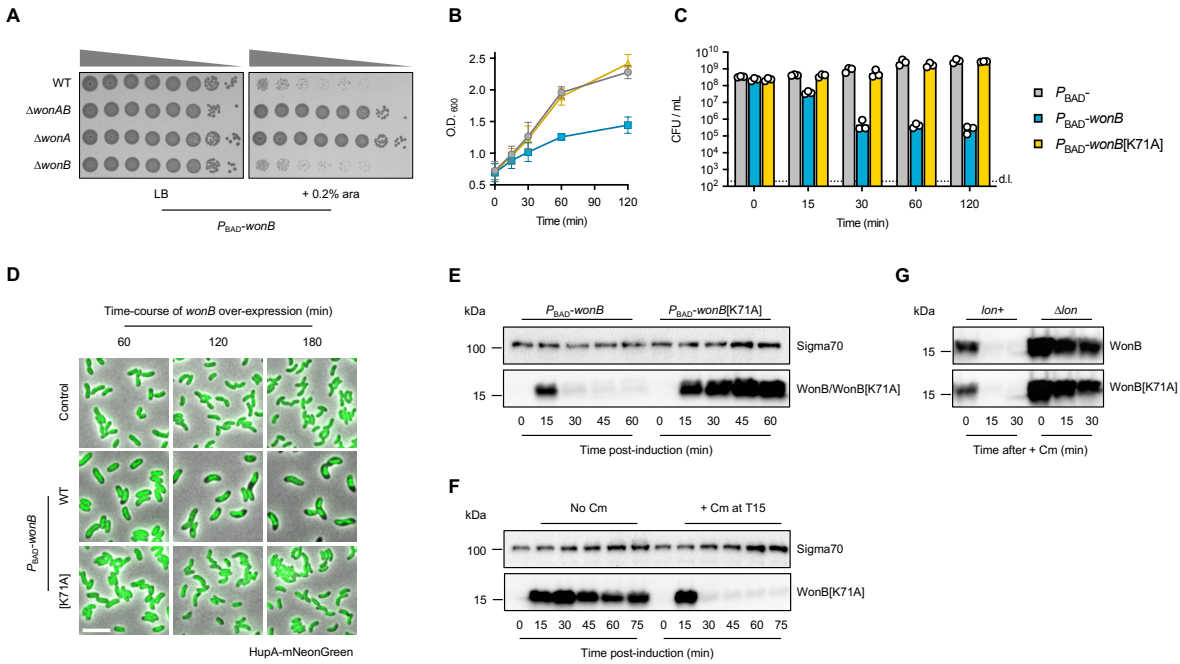

Fig. 3. WonAB activation shuts down cell growth by inhibiting translation. (**A**) Toxicity assay evaluating the growth of 10-fold serial dilutions of *V. cholerae* strain A1552 cultures and the indicated derivatives on solid media, in the absence (LB) and presence (+ 0.2% ara) of WonB overproduction. (**B-C**) Toxicity assay evaluating the growth kinetics (**B**) and cell viability (**C**) of exponentially growing cultures in liquid media upon WonB overproduction following induction at time 0, as compared to a negative control strain and a strain overproducing the inactive WonB[K71A] variant. (**D**) Time-course microscopy snapshots showing the effect of WonB overproduction on cell morphology and cellular DNA content, as monitored by a HupA-mNeonGreen fusion, compared to a negative control strain and a strain overproducing the inactive WonB[K71A] variant. Scale bar = 5 µm. (**E**) Western blot showing protein levels of WonB and WonB[K71A] over time following induction in exponentially growing cells at time 0. Predicted molecular mass of WonB, 16.1 kDa. Sigma70, was used as a loading control (**F**) Western blot showing protein levels of WonB[K71A] over time following induction in exponentially growing cells at time 0, in the absence and presence of chloramphenicol (Cm), added at 15min (T15). (**G**) Western blot showing protein levels of WonB and WonB[K71A] over time following chloramphenicol (Cm) addition, in the presence (*lon*+) and absence of Lon protease (Δ*lon*). Overexpression of genes in (**a**-**g**) was done from a chromosomally integrated transposon carrying the arabinose-inducible P_{BAD}- promoter, induced by the addition of 0.2% arabinose. Charts show mean values, error bars show s.d. All images, charts and blots are representative of the results of three independent experiments.

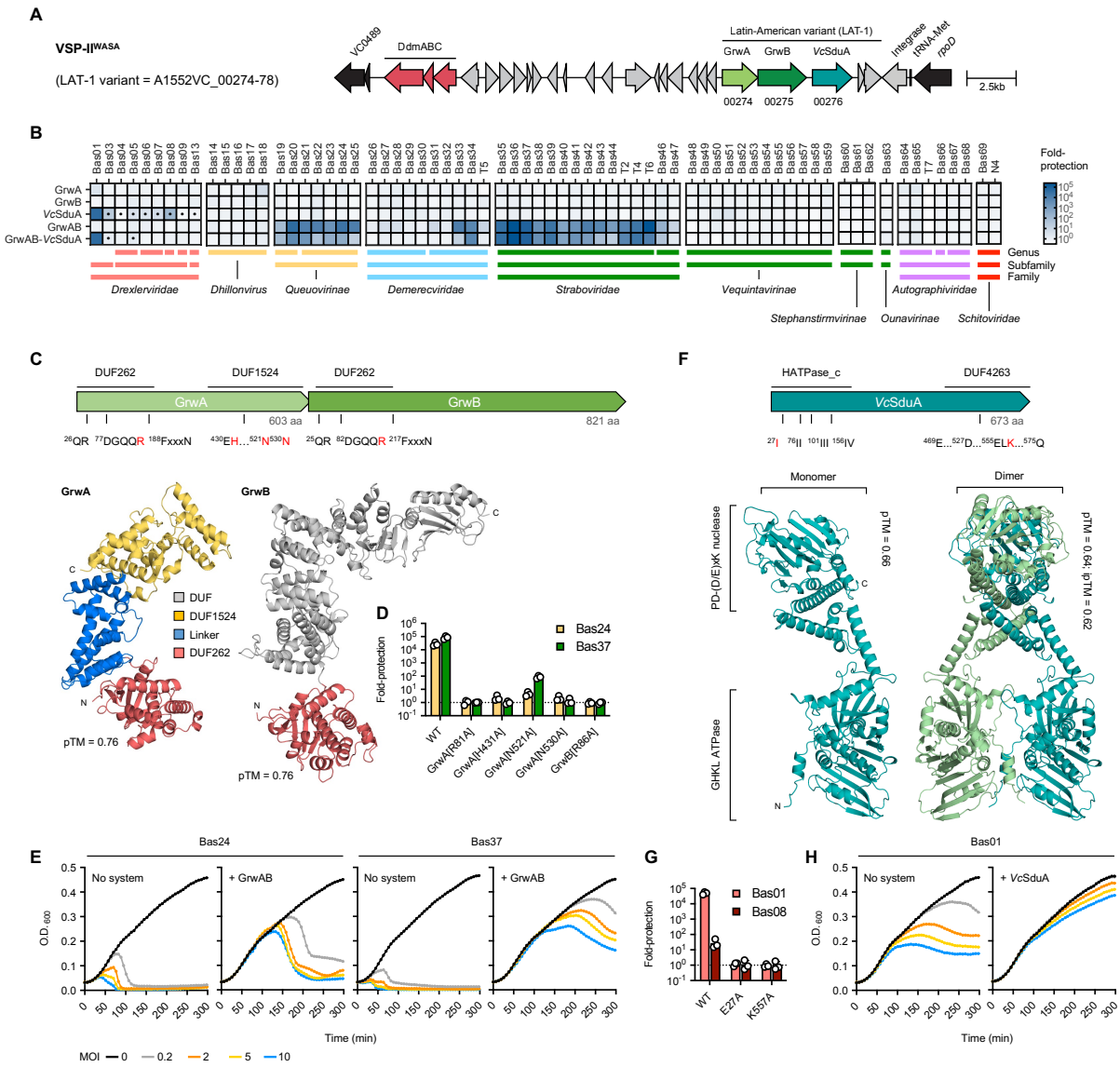

Fig. 4. VSP-II^{WASA} variant encodes two distinct anti-phage defence systems. (**A**) Schematic of VSP-II^{WASA} highlighting the LAT-1 variant present in the WASA lineage and the previously characterised DdmABC system. (**B**) Fold-protection against *E. coli* phages of the BASEL collection conferred by the production of the indicated systems and components in *E. coli*, compared to a negative 'no system' control. Boxes with a filled dot indicate phages exhibiting altered plaque morphology. Data represent the mean of two independent repeats. (**C, F**) Predicted structures of GrwAB (**C**) and *Vc*SduA (**F**) generated using AlphaFold3 shown below schematics (top) indicating the conserved domains and motifs identified in each system. Residues targeted by site-directed mutagenesis are highlighted in red. (**D, G**) Fold-protection against the indicated *E. coli* phages conferred by site-directed variants of GrwAB (**D**) and *Vc*SduA (**G**) in *E. coli*, compared to a negative 'no system' control. Bar charts show the mean + s.d. of three independent repeats. (**E, H**) Growth kinetics of *E. coli* cultures in the absence (No system) and presence of either GrwAB (**E**) or *Vc*SduA (**H**), with either no phage or infected at time 0 with the indicated MOI. Data are representative of three independent repeats. Systems were expressed from a chromosomally integrated transposon using the arabinose-inducible P_{BAD}- promoter. Growth media were supplemented with 0.2% arabinose.

1087 **Supplementary Tables**

1088 **Table S1**. Summary of defence systems predicted by DefenseFinder and PADLOC.

1089

1090 **Table S2**. Summary of WASA-1 hits detected by BLAST.

1091

1092 **Table S3**. Summary of matching hits for the *Vibrio cholerae* WonAB and *Anaerovibrio lipolyticus* OLD-

1093 ABC ATPase + Novel REase models, detected by MacSyFinder v.2.1.1.

1094

1095 **Table S4**. Summary of matching hits for the *Vibrio cholerae* GrwAB model detected by MacSyFinder

1096 v.2.1.1.

1097

1098 **Table S5**. Summary of matching hits for the *Vibrio cholerae Vc*SduA model detected by MacSyFinder

1099 v.2.1.1.

1100

1101 **Table S6**. Bacterial strains, plasmids, bacteriophages and defence systems used in this work.

1102 **Supplementary Movies**

1103 **Movie S1**. Time-lapse microscopy of ICP1 infection.

1104 Time-lapse microscopy comparing exponentially growing cells of *V. cholerae* A1552 WT and ΔWASA-

1105 1 strains after infection with ICP1-2006 at MOI 5. Cells were grown at 37°C on LB agarose and imaged

1106 automatically at 1 minute intervals for 60 minutes. Bar = 20 µm. Playback = 5 fps.

1107

1108 **Movie S2**. Time-lapse microscopy of Bas24 infection.

1109 Time-lapse microscopy comparing exponentially growing cells of *E. coli* MG1655Δ*araCBAD* in the

1110 absence (No system) and presence of GrwAB (+ GrwAB) production, after infection with Bas24 at MOI

1111 10. Cells were grown at 37°C on LB agarose + 5mM $CaCl_2$, 20mM $MgSO_4$, 0.2% arabinose and imaged

1112 automatically at 1 minute intervals for 180 minutes. Bar = 20 µm. Playback = 5 fps.